Controlling the work hardening of martensite to increase the strength/ductility balance in quenched and partitioned steels

Findley, K.O.; Hidalgo Garcia, J.; Huizenga, R. M.; Santofimia Navarro, Maria

DOI
10.1016/j.matdes.2016.12.065

Publication date
2017

Document Version
Final published version

Published in
Materials & Design

Materials and Design 117 (2017) 248–256

Contents lists available at ScienceDirect

Materials and Design

journal homepage: www.elsevier.com/locate/matdes

Controlling the work hardening of martensite to increase the strength/ductility balance in quenched and partitioned steels

K.O. Findley [b,*], J. Hidalgo [a], R.M. Huizenga [a], M.J. Santofimia [a]

[a] Department of Materials Science and Engineering, Delft University of Technology, Mekelweg 2, 2628 CD Delft, The Netherlands
[b] G.S. Ansell Department of Metallurgical and Materials Engineering, Colorado School of Mines, Golden, CO, USA

HIGHLIGHTS

- Martensite tempering was varied in a quenched and partitioned steel.
- Work hardening behavior at small strains depends on martensite dislocation density.
- Tensile ductility is impacted by small strain work hardening rate in Q&P steels.
- The strength of martensite in Q&P steels is reduced due to carbon partitioning.

GRAPHICAL ABSTRACT

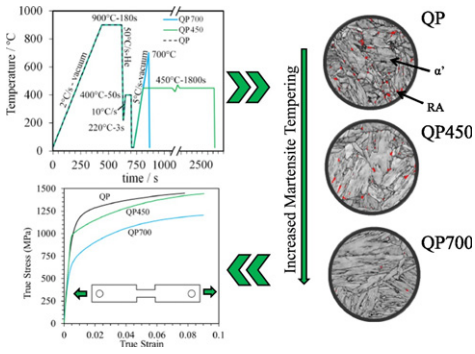

ARTICLE INFO

Article history:
Received 6 September 2016
Received in revised form 21 December 2016
Accepted 22 December 2016
Available online 24 December 2016

Keywords:
Quenching and partitioning
Tempered martensite
Retained austenite
Mechanical behavior

ABSTRACT

The role of retained austenite on tensile behavior in quenched and partitioned (Q&P) steels has been studied extensively, but the deformation behavior of martensite, which comprises the majority of Q&P microstructures, has received less attention. In this investigation, martensite properties were varied through heat treatment in a low carbon Q&P steel consisting of retained austenite and martensite. Additional conditions were produced by reheating the Q&P steel to 450 °C for 30 min or to 700 °C followed immediately by quenching. The reheated microstructures contained similar fractions of retained austenite as the non-reheated Q&P microstructures, but reheating tempered the martensite, thereby decreasing martensite dislocation density. The reheated conditions had a lower yield stress and initial work hardening rate than the non-reheated Q&P condition. However, the reheated conditions had a greater work hardening rate at larger strains and greater uniform strain due to less stable retained austenite. Furthermore, the tensile strength of the condition reheated to 450 °C was nearly equal to the non-reheated condition. In addition to retained austenite to martensite transformation, the early stage work hardening rate of martensite is critical to ductility and is dependent on martensite dislocation density, which can be decreased through tempering.

1. Introduction

Combinations of retained austenite and martensite have been predicted and experimentally shown to produce properties desired for third generation advanced high strength sheet steels (AHSS) [1].

* Corresponding author.
E-mail address: kfindley@mines.edu (K.O. Findley).

http://dx.doi.org/10.1016/j.matdes.2016.12.065

Matlock et al. [1] showed that austenite stability is also a critical factor in flow behavior through a composite model that incorporated austenite and martensite fractions as well as austenite stability. The model assumes isostrain conditions and sufficient interfacial bonding between the phases to avoid debonding. The work hardening behavior of the composite, controlled by increases in dislocation density and retained austenite to martensite transformation, results in a larger uniform strain than that achieved in the harder martensite by itself. The result is enhanced combinations of strength and ductility, specifically uniform elongation.

Uniform elongation is related to the work hardening rate through the instability criterion for necking:

$$\frac{d\sigma}{d\varepsilon} = \sigma \tag{1}$$

where σ is true stress and ε is true strain. Matlock et al. [1] noted the importance of strain hardening rate as a function of strain on uniform elongation. A high strain hardening rate at low strains has a similar effect as a high yield strength; both result in reaching the instability criterion at lower strain values, i.e. lower ductility. Therefore, it is advantageous for ductility to maintain high strain hardening rates at large strain values. Retained austenite stability directly influences the strain hardening rate as a function of strain, in turn affecting the uniform elongation that can be achieved. The high initial work hardening rate in martensite is also an important factor in composite austenite-martensite microstructures but has not yet been considered in great detail.

Microstructures containing mixtures of austenite and martensite can be produced through the quenching and partitioning (Q&P) process [2,3]. The process is performed by first austenitizing and then quenching to a temperature below the martensite start temperature to form a mixed austenite-martensite microstructure. Then, a holding step at the quench temperature or a slightly elevated temperature allows for carbon partitioning from martensite to austenite and stabilization of the remaining austenite before a final quench. The resulting microstructure consists of austenite, martensite that formed during the initial quench and was subsequently tempered in the partitioning stage, and martensite that formed during the final quench. Carbon partitioning to austenite is critical to stabilize austenite before the final quench and also to provide increased stabilization against mechanical formation of martensite during plastic deformation [3–9]. Since austenite stability is one factor that controls uniform elongation, much of the research on the Q&P process has focused on optimizing the fraction and stability of retained austenite through variations in the quench and partitioning step temperatures and times [10–14].

Tempering after the final quench is another route that can modify the austenite-martensite microstructure. Most of the work on tempering of Q&P steels has been performed on alloys with microalloy additions to obtain precipitate strengthening during the tempering step; it is proposed that these carbides can also be used to control carbon distribution [14–18]. Tempering can also change the deformation behavior and strength of the microconstituents, especially the martensite. Changes in the strength of the martensite and austenite would be expected to result in changes in the composite flow behavior. Additionally, tempering could promote diffusion of carbon from martensite to austenite as well as austenite decomposition into ferrite and carbides. These and other changes in the microstructure can have prominent effects on deformation and flow behavior.

This paper explores the effects of reheating or tempering heat treatments on tensile properties of a quenched and partitioned steel, with a focus on the possibility of engineering the strain hardening rate of martensite to alter tensile deformation response, while the initial amount of retained austenite does not vary significantly between conditions. In a previous study by Koopmans et al. [19,20] aiming to analyze the thermal stability of retained austenite in Q&P steels, a steel was subjected to various Q&P treatments and then reheated to temperatures up to 700 °C and quenched immediately. For some of the Q&P heat treatments, the reheating step resulted in little change in retained austenite volume fraction and austenite lattice parameter, implying that the austenite carbon concentration may not have significantly changed during these post Q&P heat treatments [19,20]. Thus, the alloy studied by Koopmans and the specific Q&P heat treatments that lead to minimal variations in the characteristics of the retained austenite upon heating are well suited to study the effect of tempering on martensite microstructure and its impact on tensile behavior.

2. Experimental methodology

2.1. Material and heat treatments

The composition of the steel alloy used in this study is provided in Table 1. The steel was produced using a laboratory vacuum induction furnace. After casting, the steel was hot rolled to a final thickness of 4 mm and then air cooled. Specimens with the geometry shown in Fig. 1a were machined for dilatometry heat treatments and tensile testing.

Heat treatments were performed with a Bähr 805 DIL A/D dilatometer. A type S thermocouple spot-welded on the surface was used to monitor and control temperature. A vacuum on the order of 10^{-4} mbar was used during heating or isothermal segments, and helium was used as the cooling gas. The dilatometer can be configured to heat treat a specimen as shown in Fig. 1 for subsequent tensile testing. The heat treatments are summarized in Table 2.

The baseline quench and partitioning heat treatment, labeled QP220, was previously shown [19,20] to result in a microstructure consisting of retained austenite, tempered martensite, and less than 2% as-quenched martensite; the retained austenite volume fraction was approximately 9%. Fig. 1b shows the complete thermal history. The target quench temperature of 220 °C, which varied by ±5 °C, is below the measured M_s temperature, which is 325 °C. After the heat treatment, there was 91 ± 3 vol% of martensite in the final microstructure.

Two different reheating treatments were performed on specimens initially heat treated with the QP220 heat treatment. The objective of the heat treatments was to alter the tempering conditions of the martensite while keeping the fraction of retained austenite similar to the QP220 heat treatment. One heat treatment, labeled QP220-700, consisted of the application of the heat treatment in Fig. 1b followed by a ramp in temperature to 700 °C at a rate of 5 °C/s, and then an immediate quench to room temperature. The peak temperature of 700 °C is above the Ae_1 temperature, which is approximately 637 ± 12 °C in this alloy. This heat treatment was shown by Koopmans to result in a 1–2% decrease in the fraction of retained austenite including the complete disappearance of the larger and blockier retained austenite grains [19,20]. Furthermore, the austenite lattice parameter was similar to the QP220 condition. This latter result indicates the chemical composition of the retained austenite in the QP220 and QP220-700 conditions are similar. Significant tempering of the martensite presumably occurred during the 700 °C reheating step. There is also the possibility of ferrite to austenite reversion during reheating since the peak temperature is above the A_{e1} temperature. However, the dilatometry results do not indicate any significant formation of austenite upon heating or austenite to martensite formation upon quenching from the peak temperature.

An alternative reheating treatment, labeled QP220-450 was performed as indicated in Fig. 1b and was designed to provide tempering of the martensite but to a lesser extent than the QP220-700 condition.

Table 1
Composition, in wt%, of the steel alloy used in the study.

C	Mn	Si	Mo	Al	S	P	Fe
0.20	3.51	1.525	0.509	0.03	0.0079	0.006	Balance

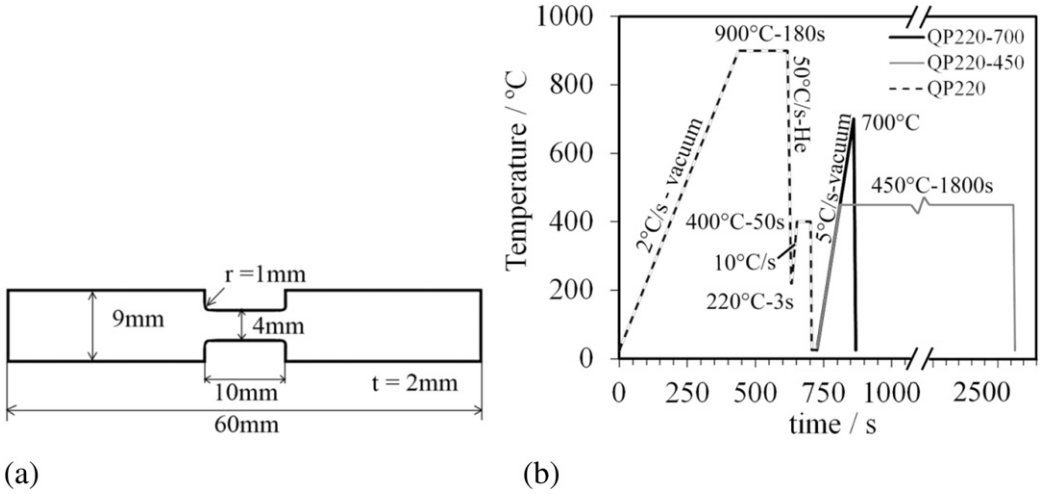

Fig. 1. (a) Geometry of specimens used for dilatometry heat treatments and tensile testing. (b) Thermal history of the QP220 heat treatment and subsequent reheating of QP220-450 and QP-700.

The heat treatment included a reheat step to 450 °C with a hold of 30 min. This heat treatment was also based on the work of Koopmans et al. [19,20] who showed that specimens from the selected alloy reheated following the QP220 treatment showed little change in austenite fraction upon reheating to temperatures up to 500 °C.

In order to compare the degree of tempering in the martensite phase in each condition, the same heat treatments were employed except the first quench temperature was reduced to 25 °C to form an as-quenched martensitic microstructure with the likely presence of a very small fraction of retained austenite. The rest of the thermal history was identical to the subsequent steps of the QP220 heat treatment in the condition labeled QP25. Similarly, the effects of the reheating steps were simulated by performing the QP25 heat treatment and then reheating to 450 or 700 °C for the same times as the QP220-450 and QP220-700 conditions; these conditions are labeled QP25-450 and QP25-700, respectively.

2.2. Tensile testing

Tensile tests were performed on all heat treatment conditions with an Instron testing frame and an extensometer with a 7.8 mm gauge length. An engineering strain rate of 0.0009/s was applied. Tensile specimens were either pulled until failure or in the case of the QP220 conditions, some tests were interrupted at various strain levels before the onset of instability to evaluate retained austenite fractions as a function of strain. Multiple tests were performed on the QP220 conditions, and good repeatability was observed in the tensile behavior. One test to failure was conducted on each of the QP25 conditions.

2.3. Characterization

Both non-strained and strained specimens were polished down to 1 μm diamond for metallographic analysis and X-Ray diffraction characterization. Scanning electron microscope (SEM) secondary electron images were obtained on QP220 specimens etched with 2% nital using a JEOL JSM-6500F field emission gun scanning electron microscope (FEG-SEM) operating at 15 kV. For the EBSD analysis, an Oxford Instruments Nordlys II detector mounted in the same microscope was used. The acceleration voltage was 20 kV, the beam current 1.2 nA, the working distance was 25 mm, the tilt angle was 70°, and the step size was 50 nm. Acquisition and post processing of Kikuchi patterns were performed with Oxford Instruments Channel 5 software.

X-Ray Diffraction experiments were carried out to estimate the volume fraction, the lattice parameter, and dislocation density of different phases after heat treatments. A Bruker D8 Advance Diffractometer equipped with a Vantec position sensitive detector was used with Co Kα radiation, an acceleration voltage of 45 kV and a current of 35 mA, while the sample was spinning at 30 rpm. The measurements were performed in the diffraction angle (2θ) range of 40°-130°, using a step size of 0.042° 2θ, with a counting time per step of 3 s. This 2θ range covers the {110}α, {200}α, {211}α,{220}α and the {111}γ, {200}γ, {220}γ, {311}γ reflections. The volume fraction of retained austenite and the errors in determining the retained austenite fraction were calculated by the direct comparison method of aforementioned austenite and martensite peaks using the procedure described by Jatczak [21]. The x-ray full width half maximum (FWHM) values of martensite peaks were used to determine dislocation density of the tempered martensite, using the modified Williamson-Hall method as detailed by HajyAkbary [22]. The Nelson-Riley method [23] was used to determine the lattice parameter in order to calculate the carbon concentration in tempered martensite, $\chi_{C\alpha'}$, using [24]:

$$\chi_{C\alpha'} = 31\ \text{wt\%}/\text{Å} \cdot (a_{\alpha'} - a_{\alpha}) \tag{2}$$

where $a_{\alpha'}$ is the lattice parameter of martensite and $a_{\alpha} = 2.866$ Å is the lattice parameter of a reference sample [25]. The effect of other alloying elements such as manganese and silicon was not considered. The carbon concentration within the austenite, $\chi_{C\gamma}$, was determined from its lattice parameter a_{γ}, (in Å) as [26]:

$$a_{\gamma} = 3.556 + 0.0453\chi_C + 0.00095\chi_{Mn} + 0.0056\chi_{Al} \tag{3}$$

where x_i, in wt% represents the concentration of the alloying element i.

Table 2
Summary of heat treatment conditions performed on the as-received steel alloy.

Condition	Heat treatment
QP220	Austenitize at 900 °C/180 s + Quench to 220 °C + Partition 400 °C/50 s + Quench
QP220-700	QP220 + Reheat to 700 °C + quench
QP220-450	QP220 + Reheat to 450 °C/30 min + quench
QP25	Austenitize at 900 °C/180 s + Quench to 25 °C + Tempering at 400 °C/50 s, and quench
QP25-700	QP25 + Reheat to 700 °C + quench
QP25-450	QP25 + Reheat to 450 °C/30 min + quench

3. Results

3.1. Initial microstructures

A representative SEM image of the quenched and partitioned steel microstructure in QP220 is shown in Fig. 2a. There is little difference between SEM images of the different conditions; they are all composed primarily of fine lath martensitic microstructures. Notably, the fine tempered martensite microstructure was even retained in the QP220-700 condition. EBSD image quality maps with retained austenite highlighted in red are provided in Fig. 2(b)–(d). There are blocky austenite grains in the QP220 and QP220-450 conditions, but the amount of these blocky austenite grains is substantially less in the QP220-700 condition. Presumably, there are also thin films of retained austenite present in all of the conditions. The presence of austenite was verified by x-ray diffraction. The image quality maps also indicate that all conditions have fine martensitic microstructures.

X-ray diffraction was used to calculate volume fractions of retained austenite, lattice parameter and carbon content of martensite, and dislocation density of martensite. Representative XRD patterns and insets of specific BCC peaks for comparison are provided in Fig. 3 for both the QP220 and QP25 conditions. The results are presented in Table 3. While the reheating step of the QP220-450 condition only slightly decreased the martensite dislocation density with respect to specimen QP220, the reheating step to 700 °C of the QP220-700 condition significantly reduced the martensite dislocation density compared to the QP220 condition. The dislocation densities in the QP25, QP25-450, and QP25-700 conditions are also shown in Table 3 and will be discussed later. The carbon concentration in martensite of the equivalent as-quenched and tempered conditions (QP25 conditions) is similar to the QP220, QP220-450, and QP220-700 conditions.

3.2. Tensile properties

Tabulated values of 0.2% offset yield strength (YS), ultimate tensile strength (UTS), uniform elongation (ε_u), and total elongation (ε_t) for all conditions are provided in Table 4. The QP220 condition exhibits a yield strength near 1000 MPa, an ultimate tensile strength of 1339 MPa, and a uniform elongation value of 8.8%. Reheating the QP220 alloy to 700 °C (QP220-700) substantially reduces the yield strength to near 700 MPa and the ultimate tensile strength to 1093 MPa; however, the uniform elongation is unchanged with respect to the QP220 condition. The QP220-450 exhibits comparable strength levels to the QP220 condition with a yield strength again near 1000 MPa and a slightly lower ultimate tensile strength of 1317 MPa compared to QP220. The uniform elongation of 9.7% for the QP220-450 condition is slightly higher than the other two conditions.

Engineering and true stress-strain curves of the QP220 conditions are shown in Fig. 4a and b. The QP220 conditions have different work hardening behavior as shown by both the engineering and true stress-strain curves in Fig. 4. For example, while the QP220-450 condition has similar tensile properties to the QP220 condition, the flow strengths between the yield strength and tensile strength are lower for the QP220-450 condition due to differences in work hardening behavior. It is interesting to observe that similar tensile properties (strength, elongation) can be achieved in a single QP steel composition but with very different tensile flow behavior. Both the QP220-450 and QP220-700 conditions clearly have higher work hardening rates than the QP220

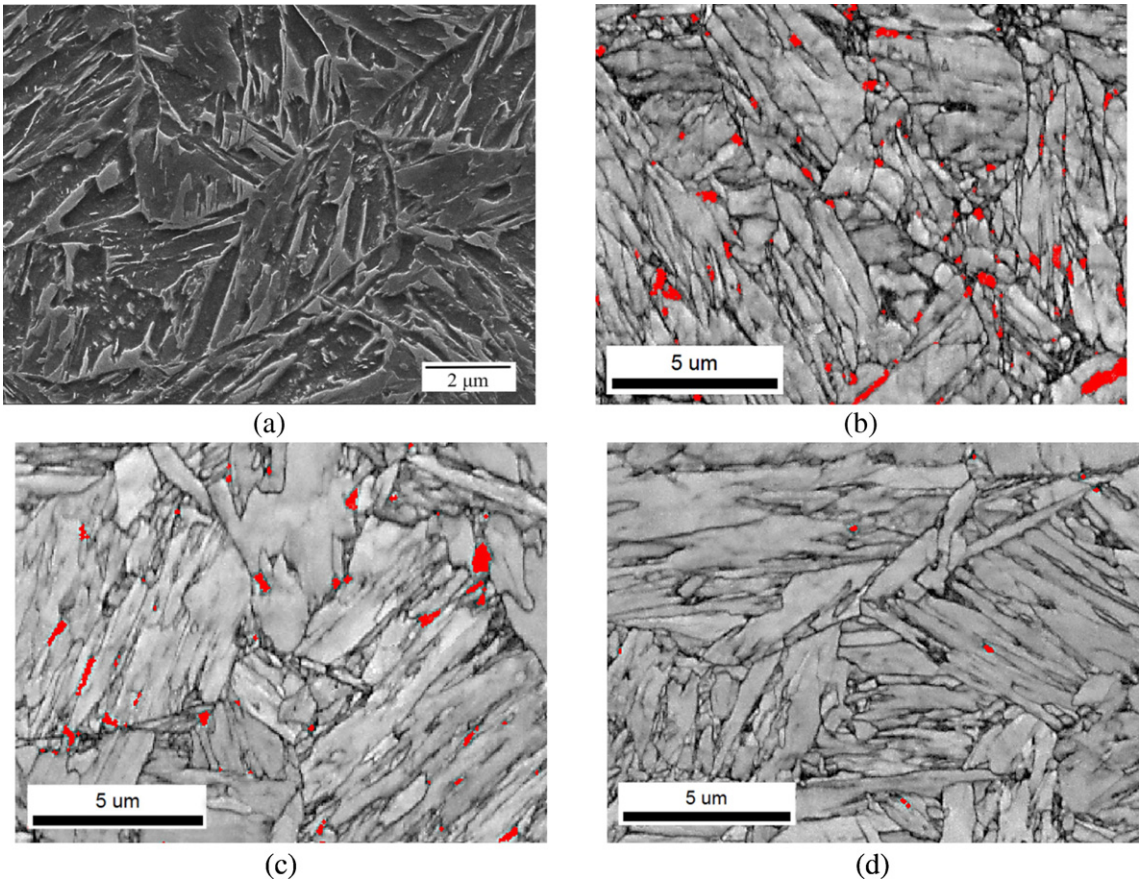

Fig. 2. Representative micrographs of QP220 conditions: (a) SEM micrograph of QP220; (b)–(d) EBSD image quality map with retained austenite highlighted red for (b) QP220, (c) QP220-450, and (d) QP220-700.

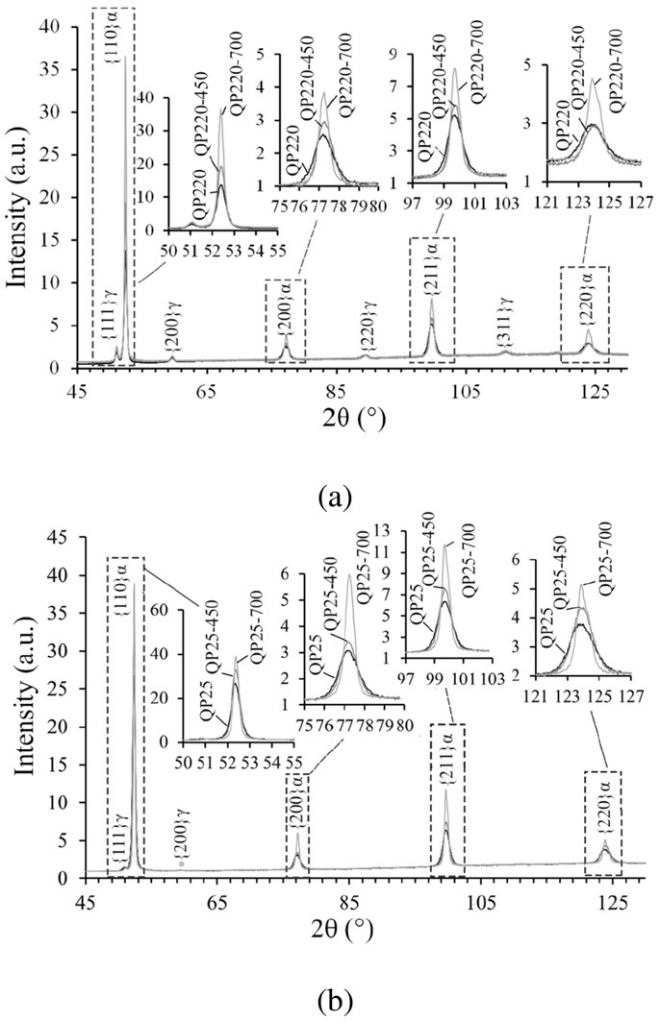

Fig. 3. Representative XRD patterns for (a) the QP220 conditions and (b) the QP25 conditions.

condition at true strains greater than 0.015 up to the point of tensile instability.

4. Discussion

The tensile flow behavior of the three QP220 alloys is affected by both retained austenite stability and work hardening behavior of austenite and martensite. As will be shown, martensite has the largest influence in the early stages of plastic deformation, while retained austenite to martensite transformation has a stronger influence in the subsequent stages of deformation. Fig. 5a shows the work hardening rate as a function of true plastic strain for all three alloys on a log-log scale to emphasize the low strain values of work hardening rate, while Fig. 5b shows the same plot on a log-linear scale to emphasize the larger strain values. Aside from the work hardening rate behavior near the yield point, the QP220 condition has the largest work hardening rate in the early stages of deformation. After a true strain of approximately 0.015, the work hardening rate of the QP220-700 and QP220-450 conditions becomes larger than that of QP220.

The fraction of retained austenite at several interrupted strain levels is shown in Fig. 6. The fraction of retained austenite decreases most rapidly at small strains for all three QP220 conditions, but the rate of transformation in the QP220 condition is smaller than the other two conditions. Thus, the higher initial work hardening rate in QP220 cannot be due to a higher rate of retained austenite to martensite transformation. All three alloys have similar amounts of carbon in austenite as shown in Table 3. Therefore, it is interpreted that the difference in austenite stability between the conditions is due to the differences in strength in the surrounding martensite phase, which is presented in more detail in a separate publication [27].

The difference in work hardening rate between the QP220 conditions is due to differences in the martensitic microstructure. To further emphasize this point, Fig. 7 shows the work hardening rate as a function of true strain for the specimens that were heat treated to compare the amount of tempering in the martensite during the heat treatments: QP25, QP25-450, and QP25-700. The QP25 condition, representing the martensite in the QP220 condition, has the largest work hardening rate up to true strains slightly past 0.02. As can be seen in Table 3, the QP25 condition also has the highest dislocation density of all the QP25 conditions. In the early stages of deformation, the work hardening rate of this condition is high because of the large number of dislocation-dislocation interactions, leading to the micro-yielding behavior typical of as-quenched or lightly tempered lath martensitic steels. This micro-yielding behavior is also the likely reason for the initial high work hardening rate in the QP220 condition.

The degree of retained austenite to martensite transformation is much greater during deformation of the QP220-450 and QP220-700 conditions than the QP220 condition. In fact, nearly all of the retained austenite transforms to martensite in the QP220-700 condition at less than 0.03 true strain, while approximately 6–7% of retained austenite transforms to martensite in the QP220-450 condition compared to 4% for the QP220 condition. This lower austenite stability correlates to the higher work hardening rate in the QP220-450 and QP220-700 conditions past a true strain of approximately 0.015 as more fresh martensite forms, which contributes to work hardening. In contrast, retained austenite transforms more gradually in the QP220 condition, resulting in a lower work hardening rate at higher strains. However, even in the QP220 condition, retained austenite to martensite transformation has an influence on the work hardening behavior, which can be observed by comparing the work hardening rate as a function of strain for the QP220 and QP25 conditions. The work hardening rate of the QP25 condition drops steadily to approximately 1550 MPa at a true strain of 0.04, while the rate of decrease in work hardening rate is lower in QP220 as a function of strain and is above 3000 MPa at a true strain of 0.04. Overall, the work hardening rate of all three QP220 conditions is substantially greater than their QP25 counterparts at true strains greater than 0.015.

The tensile behavior of the QP220 and corollary QP25 conditions is compared more directly in Fig. 8. Fig. 8(a) shows the engineering stress-strain behavior of the QP220 and QP25 conditions. The primarily tempered martensite microstructure of the QP25 condition results in a higher UTS than the QP220 condition. The QP25 tensile data can be

Table 3
Austenite volume fraction ($V_f(\gamma)$), carbon content of austenite ($\chi_{C\gamma}$), martensite dislocation density (ρ_{dis}), carbon content of martensite ($\chi_{C\alpha'}$), and estimated volume fraction of Fe_3C precipitates (V_f (carbide)) of the QP220 and QP25 conditions before straining. In the QP25 conditions, it is assumed that no austenite is present in the final microstructure.

	QP220	QP220-450	QP220-700	QP25	QP25-450	QP25-700
$V_f(\gamma)$ [%]	9 ± 3	10 ± 3	6.2 ± 1.5	–	–	–
$\chi_{C\gamma}$ [wt%]	0.91 ± 0.5	0.88 ± 0.5	0.89 ± 0.5	–	–	–
$\rho_{dis.}$ [10^{15} m^{-2}]	3.1 ± 0.5	2.1 ± 0.4	0.5 ± 0.2	3.1 ± 0.4	2.3 ± 0.3	0.6 ± 0.2
$\chi_{C\alpha'}$ [wt%]	0.11 ± 0.03	0.08 ± 0.02	0.04 ± 0.01	0.11 ± 0.03	0.07 ± 0.03	0.05 ± 0.01
V_f (carbide) [%]	0.3 ± 0.9	0.7 ± 0.9	1.8 ± 0.8	1.5 ± 0.9	2.2 ± 0.9	2.5 ± 0.9

Table 4
Average and standard deviation of tensile properties of the studied materials obtained from the engineering stress-strain curves. The standard deviation of the total elongation of the QP220 condition is not reported because of extensometer slippage in all but one specimen in the post-uniform elongation region but is likely less than 2% based on the results from the other conditions. One test was performed on each of the QP25 conditions.

	QP220	QP220-450	QP220-700	QP25	QP25-450	QP25-700
YS (MPa)	999 ± 50	1006 ± 10	697 ± 40	1203	1114	920
UTS (MPa)	1339 ± 4	1317 ± 2	1093 ± 10	1480	1317	1033
ε_u (%)	8.8 ± 0.8	9.7 ± 0.3	8.8 ± 0.7	4.1	5.6	7.4
ε_t (%)	21.9	23.6 ± 0.2	22.4 ± 1.5	20.5	18.1	23.9

used to represent martensite in a composite model of the flow stress of the QP220 condition, which initially contains approximately 91 vol% martensite and 9 vol% austenite. However, the QP25 data provides a vast overestimate of the flow properties of the QP220 condition. For example, at a strain of 3%, the flow strength of the QP25 condition is 1475 MPa. Assuming isostrain behavior and approximately 90 vol% martensite, the martensite would contribute 1328 MPa to the flow strength, which is larger than the flow strength of 1295 MPa of QP220 at 3% strain. In other words, the strength of the QP220 condition would be overestimated even without accounting for the austenite contribution to strength. This analysis suggests that the martensite in the QP220 condition is not as strong as the martensite in the QP25 condition in which the 50 s tempering heat treatment was meant to simulate the partitioning component of the QP220 thermal history.

The XRD results in Table 3 indicate that the dislocation density and solute carbon are similar in martensite in the QP25 and QP220 conditions. Therefore, it is interpreted that the difference in martensite strength is due to differences in carbide precipitation. In the QP25 condition, there is 0.11 wt% carbon in solution, leaving 0.09 wt% carbon for carbide precipitates. Similarly, there is 0.11 wt% carbon in solution in martensite in the QP220 condition but the remaining carbon is divided between austenite and carbides in the martensite. The XRD results reveal that indeed there is 0.91 wt% carbon in the austenite in QP220. Using a lever rule calculation with the remaining solute content in martensite in each condition and assuming zero solubility for carbon in ferrite, the volume fraction of carbides is approximately 0.015 in the QP25 condition and 0.003 in the QP220 condition (Table 3). The SEM image in Fig. 9 shows that the amount of carbide precipitation is significantly higher in QP25 than in QP220 (Fig. 2a). The strengthening contribution of these precipitates can be estimated using Gladman's equation for Orowan looping of dislocations around precipitates in polycrystalline alloys [28]:

$$\Delta\sigma_y = \left(0.538Gbf^{1/2}/X\right)\ \ln(X/2b) \tag{4}$$

where $\Delta\sigma_y$ is the increase in yield strength, G is the shear modulus, b is the Burgers vector, f is the volume fraction of particles, and X is the real diameter of the Fe_3C precipitates. For precipitate sizes up to 100 nm, the amount of precipitate strengthening in the QP25 condition is between 80 and 150 MPa greater than the QP220 condition.

This difference in precipitate strengthening can account for the postulated strength differences in the lath martensite between the QP25 and QP220 conditions. For example, if the martensite in QP25 is 80 MPa stronger than the martensite in QP220, then the martensite strength contribution would not fully account for the flow stress observed in QP220 in a composite model. Using the flow stress of QP25 at 3% strain (1475 MPa), the flow stress of martensite in QP220 would be 1395 MPa and would contribute 1255 MPa of strength at an approximate volume fraction of 0.9 in the microstructure. The flow strength of QP220 at 3% strain is 1295 MPa. Thus, 40 MPa would have to be contributed by austenite with an approximate volume fraction of 0.1, which would imply austenite has a flow strength of approximately 400 MPa at 3% strain. It is noted that this calculation is only provided as an example and the exact contributions of each phase depend on more precise values of Fe_3C size and distribution. Overall, an important consideration for Q&P microstructural design is that the martensite strength in Q&P microstructures is less than a fully martensitic microstructure with the same alloy composition.

Fig. 8(b) shows the engineering stress-strain curves for the QP220-450 and QP25-450 conditions. Initially, the flow strength of the QP25-450 condition, with a microstructure consisting of primarily tempered martensite, is greater than that of the QP220-450 condition. Once again, the flow strength of the QP25-450 condition is initially too high to predict the martensite contribution to the QP220-450 flow strength, though the additional tempering of the QP25-450 condition compared to the QP25 condition results in a significant reduction in martensite strength. As already noted, the work hardening rate of the QP220 conditions is greater than the QP25 conditions at strains greater than 0.015. Because of this higher work hardening rate, the UTS of the QP220-450 condition is nearly equal to the UTS of the QP25-450 condition, although it is reached at higher strain values. These conditions show the importance of retained austenite to martensite transformation in maintaining

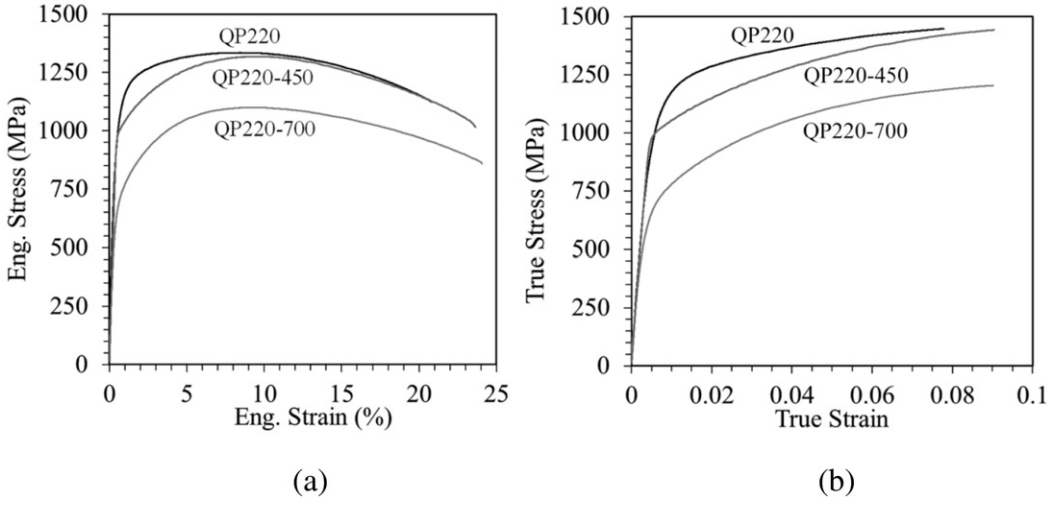

Fig. 4. (a) Engineering stress-strain curves of the three QP220 conditions. (b) True stress-strain curves for the same conditions.

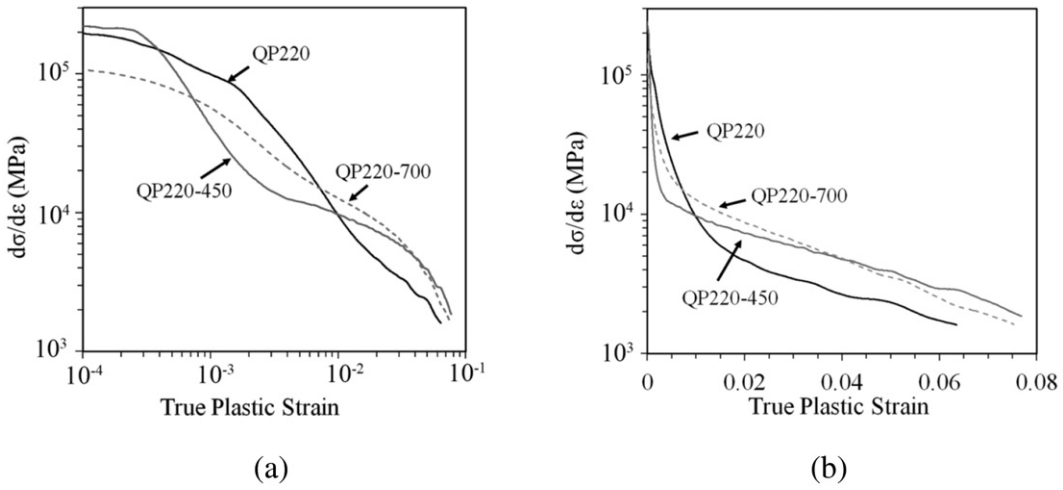

Fig. 5. Work hardening rate as a function of true strain for the QP220, QP220-450, and QP220-700 conditions: (a) log-log scale (b) linear-log scale.

a high work hardening rate and contributing to both enhanced strength and uniform elongation.

Fig. 8(c), a plot of the engineering stress-strain curves of the QP220-700 and QP25-700 conditions, more dramatically shows the influence of austenite to martensite transformation during straining. Because of the higher work hardening rate of the QP220-700 condition at larger strains, the UTS of the QP220-700 condition exceeds that of the QP25-700 condition. All three QP220 conditions show that instability is delayed compared to their QP25 counterparts. The martensite in the QP25-700 condition was heavily tempered as evident by the sharp yield point and overall lower strength compared to the other QP25 conditions.

The QP25 tempered martensitic microstructures provide important insight into the role of martensite in the work hardening behavior of Q&P steels. The QP25 and QP25-450 tensile properties demonstrate that the strength and initial work hardening rate of the martensite in the QP220-450 condition is likely less than in the QP220 condition. However, the UTS of the QP220-450 condition is nearly equal to the QP220 condition and the uniform elongation of the QP220-450 condition is greater (Table 4). These strength and ductility properties correspond to the assertion of Matlock et al. [1] that the work hardening rate as a function of strain, which is influenced by retained austenite stability, is directly related to the ultimate tensile strength and ductility of steels containing significant fractions of retained austenite. The unique observation in the present study is that the work hardening rate of the martensite can also be engineered and impacts the ductility of martensite-austenite composite microstructures. The fact that the austenite stability is greater as a function of strain in the QP220 condition should promote sustained high work hardening rates and enhanced ductility. However, the austenite to martensite transformation effects are counteracted by the initially high work hardening rate in the martensite, which leads to instability at lower strains. Although the austenite stability in the QP220-450 condition is lower, the initial work hardening rate in the QP220-450 condition is also lower due to the degree of martensite tempering. The low initial work hardening rate combined with work hardening from the austenite to martensite transformation results in a nearly equal strength and greater uniform elongation in the QP220-450 condition compared to the QP220 condition, despite differences in martensite strength between the two conditions.

5. Summary and conclusions

Reheating heat treatments were performed on a quenched and partitioned steel, which resulted in variations in martensite tempering, while preserving comparable fractions of retained austenite before deformation. An investigation of the tensile flow behavior of the alloys revealed the following:

1) Reheating quenched and partitioned steels to both 450 °C (QP220-450) and 700 °C (QP220-700) decreased retained austenite stability, which led to greater work hardening rates at true strains above

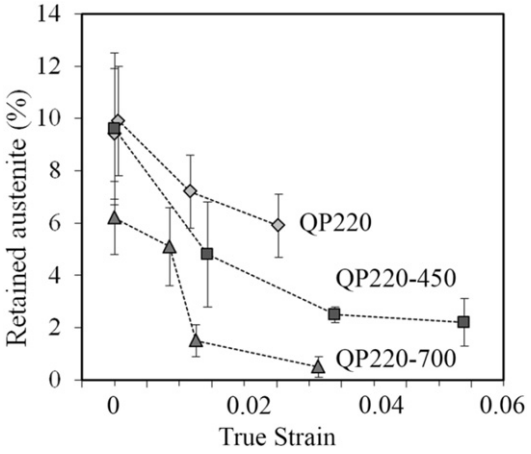

Fig. 6. Retained austenite fraction as a function of true strain for the QP220, QP220-450, and QP220-700 conditions.

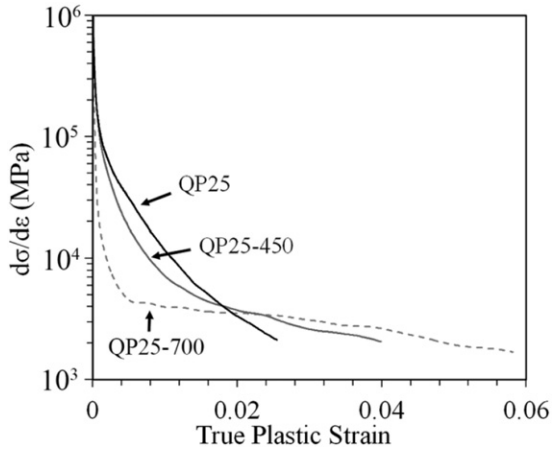

Fig. 7. Work hardening rate as a function of strain for the QP25, QP25-450, and QP25-700 conditions.

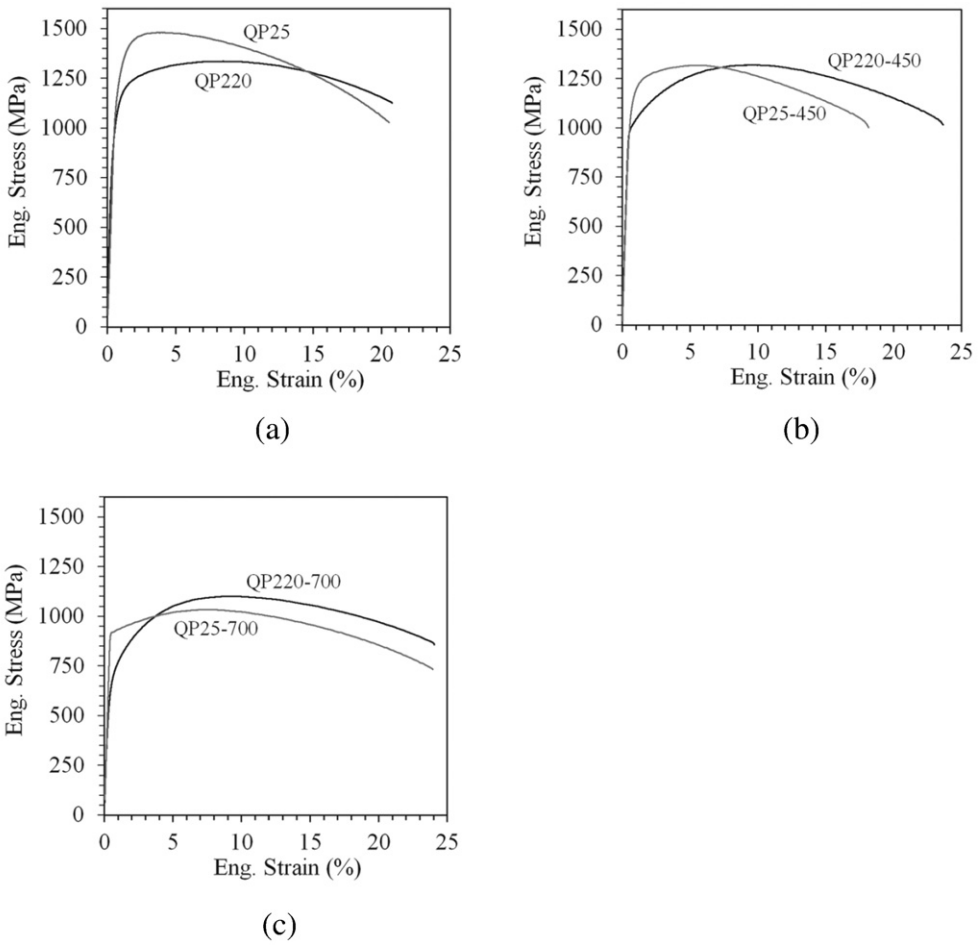

Fig. 8. Engineering stress-strain curves for (a) QP220 and QP25 conditions, (b) QP220-450 and QP25-450 conditions, and (c) QP220-700 and QP25-700 conditions.

0.015 compared to a quenched and partitioned condition without reheating (QP220). The work hardening rate in the QP220 condition was higher at small strains due to a smaller degree of tempering of the martensite in the microstructure. This difference in low-strain work hardening behavior was also observed in as-quenched martensitic microstructures (QP25 conditions) that were tempered with the same partitioning and reheating schedules as the QP220 conditions.

2) A comparison of the work hardening behavior of the QP220 and QP25 conditions at larger strains shows that the work hardening rates for the QP220 conditions are enhanced due to retained austenite to martensite transformation, which results in the UTS of the QP220-450 and QP220-700 conditions being equal to or exceeding the UTS of their QP25 counterparts.
3) While the QP25 conditions were produced to estimate changes in martensite strength due to the different thermal histories of the QP220 conditions, the strength of these tempered martensite conditions is larger than the strength of the martensite in the QP220 conditions. The strength difference is primarily due to differences in amount of carbide precipitation in martensite. The dislocation densities and solute carbon amounts are similar in martensite in the QP25 and QP220 conditions.
4) The QP220-450 condition has nearly the same UTS and slightly larger elongation than the QP220 condition despite having very different work hardening behavior. This comparison shows that the small strain work hardening behavior, which is mostly controlled by the martensite in the Q&P microstructures, can be influenced by martensite tempering. While most studies of microstructural design of Q&P steels focus on designing austenite stability for strength and ductility, this study reveals that the early stage work hardening behavior is also important and can be engineered by martensite tempering.

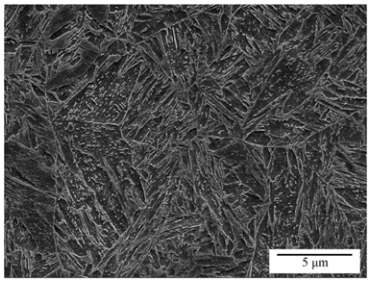

Fig. 9. SEM image of lath martensite microstructure and carbides in the QP25 condition.

Acknowledgments

The authors want to acknowledge Jilt Sietsma from the Delft University of Technology and Tjerk Koopmans from VDL for their assistance and advice on this work. The research leading to these results has received funding from the European Research Council under the European Union's Seventh Framework Programme (FP/2007-2013)/ERC Grant Agreement no. [306292]. The research also received support from support from National Science Foundation through CAREER Award No. 0955236 and the National Science Foundation/European Research Council Research Opportunities in Europe for CAREER Awardees program.

References

[1] D.K. Matlock, J.G. Speer, Third generation of AHSS: microstructure design concepts, in: A. Haldar, S. Suwas, D. Bhattacharjee (Eds.), Microstructure and Texture in Steels, Springer, London 2009, pp. 185–205.

[2] M.J. Santofimia, R.H. Petrov, L. Zhao, J. Sietsma, Microstructural analysis of martensite constituents in quenching and partitioning steels, Mater. Charact. 92 (2014) 91–95.

[3] J.G. Speer, E. De Moor, A.J. Clarke, Critical assessment 7: quenching and partitioning, Mater. Sci. Tech-Lond. 31 (2015) 3–9.

[4] J. Speer, D.K. Matlock, B.C. De Cooman, J.G. Schroth, Carbon partitioning into austenite after martensite transformation, Acta Mater. 51 (2003) 2611–2622.

[5] A.J. Clarke, J.G. Speer, M.K. Miller, R.E. Hackenberg, D.V. Edmonds, D.K. Matlock, F.C. Rizzo, K.D. Clarke, E. De Moor, Carbon partitioning to austenite from martensite or bainite during the quench and partition (Q&P) process: a critical assessment, Acta Mater. 56 (2008) 16–22.

[6] M.J. Santofimia, L. Zhao, R. Petrov, C. Kwakernaak, W.G. Sloof, J. Sietsma, Microstructural development during the quenching and partitioning process in a newly designed low-carbon steel, Acta Mater. 59 (2011) 6059–6068.

[7] M.J. Santofimia, L. Zhao, J. Sietsma, Overview of mechanisms involved during the quenching and partitioning process in steels, Metall. Trans. A 42 (2011) 3620–3626.

[8] Y. Toji, G. Miyamoto, D. Raabe, Carbon partitioning during quenching and partitioning heat treatment accompanied by carbide precipitation, Acta Mater. 86 (2015) 137–147.

[9] M. Gouné, F. Danoix, S. Allain, O. Bouaziz, Unambiguous carbon partitioning from martensite to austenite in Fe-C-Ni alloys during quenching and partitioning, Scr. Mater. 68 (2013) 1004–1007.

[10] E. De Moor, J.G. Speer, D.K. Matlock, J.H. Kwak, S.B. Lee, Effect of carbon and manganese on the quenching and partitioning response of CMnSi steels, ISIJ Int. 51 (2011) 137–144.

[11] D. De Knijf, E.P. Da Silva, C. Föjer, R. Petrov, Study of heat treatment parameters and kinetics of quenching and partitioning cycles, Mater. Sci. Tech-Lond. 31 (2015) 817–828.

[12] I. De Diego-Calderón, D. De Knijf, J.M. Molina-Aldareguia, I. Sabirov, C. Föjer, R. Petrov, Effect of Q&P parameters on microstructure development and mechanical behaviour of Q&P steels, Rev. Metal. 51 (2015).

[13] A. Arlazarov, O. Bouaziz, J.P. Masse, F. Kegel, Characterization and modeling of mechanical behavior of quenching and partitioning steels, Mater. Sci. Eng. A 620 (2015) 293–300.

[14] E. De Moor, J.G. Speer, D.K. Matlock, C. Föjer, J. Penning, Effect of Si, Al and Mo alloying on tensile properties obtained by quenching and partitioning, Materials Science and Technology Conference and Exhibition 2009, MS&T 2009, pp. 1554–1563.

[15] N. Zhong, X.D. Wang, L. Wang, Y.H. Rong, Enhancement of the mechanical properties of a Nb-microalloyed advanced high-strength steel treated by quenching-partitioning-tempering process, Mater. Sci. Eng. A 506 (2009) 111–116.

[16] X.D. Wang, N. Zhong, Y.H. Rong, T.Y. Hsu, L. Wang, Novel ultrahigh-strength nanolath martensitic steel by quenching-partitioning-tempering process, J. Mater. Res. 24 (2009) 260–267.

[17] K. Zhang, M. Zhang, Z. Guo, N. Chen, Y. Rong, A new effect of retained austenite on ductility enhancement in high-strength quenching-partitioning-tempering martensitic steel, Mater. Sci. Eng. A 528 (2011) 8486–8491.

[18] X.D. Wang, W.Z. Xu, Z.H. Guo, L. Wang, Y.H. Rong, Carbide characterization in a Nb-microalloyed advanced ultrahigh strength steel after quenching-partitioning-tempering process, Mater. Sci. Eng. A 527 (2010) 3373–3378.

[19] T.T.W. Koopmans, Thermal Stability of Retained Austenite in Quenching & Partitioning Steels(MSc Thesis) Materials Science and Engineering Department, TU Delft, Delft, 2015.

[20] T.T.W. Koopmans, J. Sietsma, M.J. Santofimia, Analysis of the Thermal Stability of Quenching and Partitioning Steel Microstructures(To be published) 2016.

[21] C.F. Jatczak, Retained Austenite and Its Measurement by X-Ray Diffraction, SAE Technical Papers, 1980.

[22] F. HajyAkbary, J. Sietsma, A.J. Böttger, M.J. Santofimia, An improved X-ray diffraction analysis method to characterize dislocation density in lath martensitic structures, Mater. Sci. Eng. A 639 (2015) 208–218.

[23] J.B. Nelson, D.P. Riley, An experimental investigation of extrapolation methods in the derivation of accurate unit-cell dimensions of crystals, Proc. Phys. Soc. 56 (1945) 160–176.

[24] B. Hutchinson, J. Hagström, O. Karlsson, D. Lindell, M. Tornberg, F. Lindberg, M. Thuvander, Microstructures and hardness of as-quenched martensites (0.1–0.5%C), Acta Mater. 59 (2011) 5845–5858.

[25] N. Ridley, H. Stuart, Lattice parameter anomalies at the curie point of pure iron, J. Phys. D. Appl. Phys. 1 (1968) 1291–1295.

[26] N.H. Van Dijk, A.M. Butt, L. Zhao, J. Sietsma, S.E. Offerman, J.P. Wright, S. Van Der Zwaag, Thermal stability of retained austenite in TRIP steels studied by synchrotron X-ray diffraction during cooling, Acta Mater. 53 (2005) 5439–5447.

[27] J. Hidalgo, K.O. Findley, M.J. Santofimia, Thermal and mechanical stability of retained austenite surrounded by martensite with different degrees of tempering, Mater. Sci. Eng. A (2016) (submitted for publication).

[28] T. Gladman, The Physical Metallurgy of Microalloyed Steels, The Institute of Materials, London, 1997.